Materials & Design 231 (2023) 112024

Contents lists available at ScienceDirect

Materials & Design

journal homepage: www.elsevier.com/locate/matdes

Suppressing hydrogen blistering in a magnesium-rich healable laser powder bed fusion aluminum alloy analyzed by in-situ high resolution techniques

Julie Gheysen [a,*], Ankush Kashiwar [a,b], Hosni Idrissi [a,b], Julie Villanova [c], Aude Simar [a]

[a] Institute of Mechanics, Materials and Civil Engineering (iMMC), Université catholique de Louvain, B-1348 Louvain-la-Neuve, Belgium
[b] Department of Physics, Electron Microscopy for Materials Science (EMAT), University of Antwerp, B-2020 Antwerpen, Belgium
[c] ESRF - The European Synchrotron, Grenoble 38043, France

HIGHLIGHTS

- A new healable aluminium alloy was developed and successfully manufactured by laser powder bed fusion.
- Heating in-situ transmission electron microscopy highlighted the healing mechanism.
- 3D X-ray nano-holotomography showed the healing of voids smaller than 500 nm diameter in magnesium-rich 4xxx series aluminum alloys.
- 3D X-ray nano-holotomography evidenced that the addition of magnesium in 4xxx series aluminum alloys suppresses the hydrogen blistering.

GRAPHICAL ABSTRACT

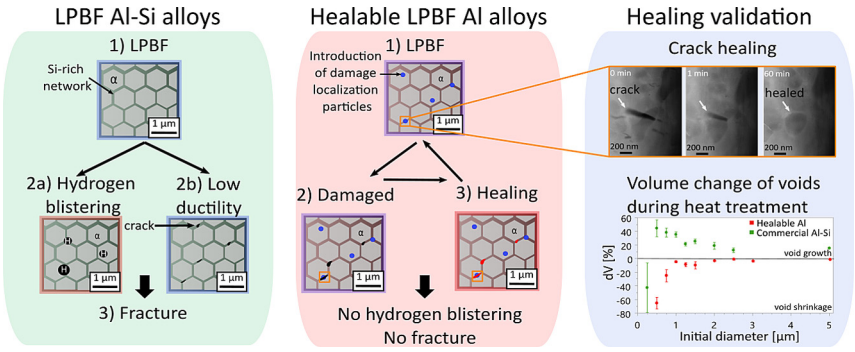

ARTICLE INFO

Article history:
Received 17 January 2023
Revised 29 April 2023
Accepted 19 May 2023
Available online 20 May 2023

Keywords:
Hydrogen blistering
Self-healing
Laser powder bed fusion (LPBF)
Aluminum alloy
Synchrotron radiation computed tomography

ABSTRACT

Hydrogen blistering, i.e. precipitation of supersaturated hydrogen at elevated temperatures, increases porosity during heat treatments in 4xxx series Al alloys manufactured by laser powder bed fusion (LPBF), as demonstrated by 3D X-ray nano-imaging in AlSi12. This paper proposes the design of a healable Al alloy to suppress hydrogen blistering and improve the damage management. The strategy consists of solute atoms diffusing towards nano-voids and precipitating on their surface, thereby filling the damage sites. A new healable Al alloy was thus developed and successfully manufactured by LPBF. 3D X-ray nano-imaging evidenced that the addition of Mg in 4xxx series Al alloys suppresses the hydrogen blistering. This is expectedly due to Mg in solid solution which increases the hydrogen solubility in the Al matrix and due to the healing of these hydrogen pores. Moreover, a significant healing of voids smaller than 500 nm diameter is observed. In-situ heating inside transmission electron microscopy pointed out that Al matrix diffuses inside the fractured Mg2Si particles, thereby demonstrating the healing ability of the new alloy. This has opened the doors to development of new healable Al alloys manufactured by LPBF as well as to new post-treatments to tailor mechanical properties and microstructure without hydrogen blistering.

© 2023 The Authors. Published by Elsevier Ltd. This is an open access article under the CC BY license (http://creativecommons.org/licenses/by/4.0/).

* Corresponding author.
E-mail address: julie.gheysen@epfl.ch (J. Gheysen).

https://doi.org/10.1016/j.matdes.2023.112024
0264-1275/© 2023 The Authors. Published by Elsevier Ltd.
This is an open access article under the CC BY license (http://creativecommons.org/licenses/by/4.0/).

1. Introduction

Laser powder bed fusion (LPBF) is an additive manufacturing process also formerly called selective laser melting (SLM). This technology is mainly used in aeronautic and automotive industries as it allows the manufacturing of complex and customized geometries which are not always possible by conventional manufacturing techniques [1]. Based on a computer-aided design model, a laser beam melts layer-by-layer the area of the powder bed which will compose the manufactured part [1].

Aluminum alloys are materials of choice for the aeronautics and automotive industries thanks to their excellent strength to weight ratio [2]. 4xxx series Al alloys (Al-Si) are the most commonly investigated LPBF Al alloys due to their excellent castability and low thermal expansion coefficient [3]. The high cooling rate of LPBF induces a very fine microstructure, which leads to excellent mechanical properties such as higher strength than cast alloys [4]. The resulting microstructure is composed of α-Al phase cells surrounded by a Si-rich interconnected network [5]. This Si-rich network is the source of damage nucleation and lowers the ductility of the 4xxx series LPBF Al alloys compared to conventional manufacturing technologies. One solution to increase the ductility of these Al alloys consists in applying a post-treatment such as T6, i.e. solution heat treatment (400–550 °C) followed by artificial ageing [6–8]. However, severe hydrogen blistering causes a significant increase in porosity (see Fig. 1) and thus, deteriorates the ductility [6,9]. Indeed, during LPBF, water vapor (from moisture on powder particles surfaces) or supersaturated hydrogen in the atomized powder particles [10] reacts with Al forming H^+ protons [9]. As hydrogen has a large solubility in liquid Al (0.88 ml/100 g [6]), these protons are absorbed in the melt. Solid Al exhibits a much lower solubility limit (0.06 ml/100 g [6]). Now, due to the high cooling rate of LPBF (typically 10^6 K/s [11]), this hydrogen is trapped in supersaturated solid solution in the solid Al. As the temperature increases during the post-manufacturing heat treatment, the supersaturated hydrogen trapped in the Al matrix clusters forming hydrogen gas and gathering as pores, increasing thus the porosity of the Al alloy (see Fig. 1) [6,9].

The approach proposed here to increase the damage management and to avoid the hydrogen blistering of these LPBF Al alloys is to make these LPBF Al alloys *healable*. "Self-healing" is a concept inspired by nature which is based on the notion that the formation of damage is accepted as long as it is counteracted by a process of removing this damage [12]. The development of self-healing man-made materials has been extensively studied in the past 20 years and is already commercialized for polymers. All the healing strategies are based on the same working principle: generation of a mobile phase, called healing agent, which will fill the crack [13]. The development of self-healing metallic materials is more challenging due to the low mobility of atoms at room temperature [14,15]. Therefore, an external driving force is required to promote the mass transfer of the mobile healing agent towards damage sites.

Different healable Al alloys have already been investigated where solute atoms diffuse towards nano-voids and precipitate on their surface, filling the damage sites [14,15]. Hautakangas *et al.* [16] have studied an Al-Cu-Mg alloy in underaged condition and during natural ageing. They showed that the underaged condition is required for healing as it induces a microstructure composed of alloying elements in supersaturated solid solution and provides thus, a good healing potential. Song *et al.* [17] showed the healing potential of an Al-Mg-Er alloy (with minor Mn additions). After its cold rolling step, the $AlMn_6$ precipitates are broken generating a large number of voids in the alloy. After 50 min at 180 °C, transmission electron microscopy (TEM) observations showed that these voids were successfully healed. Indeed, Mg, which has the highest diffusion rate in Al, is the first element to reach and thus fill these voids. After two hours, the rest of the matrix elements had time to diffuse and the composition of the filled voids is similar to the matrix. Arseenko *et al.* [18] developed

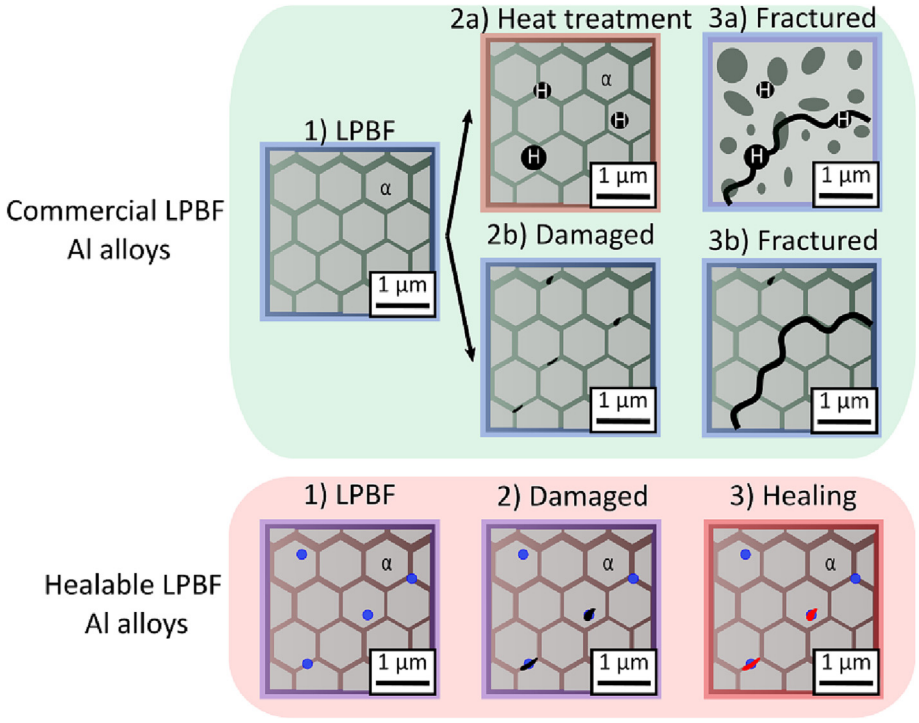

Fig. 1. Schematic of the hydrogen blistering (2a and 3a) and damage mechanism (2b and 3b) of common commercial LPBF Al alloys (green box) and the PDR strategy investigated in this paper (red box). The α-Al cells are schematized as light grey hexagons surrounded by a Si-rich network (in dark grey). Voids are drawn in black with a white H if due to hydrogen blistering, the damage localization particles are in blue and the healing agent is in red during healing.

a new healing strategy called the programmed damage and repair (PDR) healing strategy. In this strategy, Mg was incorporated in a commercial Al6063 using 16 passes of friction stir processing (FSP). Such a manufacturing route is not adapted for industrial part production. The microstructure is thus composed of Mg_2Si precipitates which are damage localization particles and Mg in solid solution in the α-Al matrix available as healing agent to precipitate inside voids. The novelty of this PDR strategy relies on the control of the size of damage localization Mg_2Si particles in order to keep it below the maximum void size that can be healed and thus, ensuring that the voids can be healed. In-situ heating coupled to X-ray nano-holo-tomography (nano-CT) highlighted the disappearance of 90 % of the smallest voids initiated by the fracture of Mg_2Si particles (below 200 nm) and the progressive filling of larger ones after a healing heat treatment (HHT) at 400 °C during 10 min.

In common 4xxx series LPBF Al alloys, i.e. composed of α-Al cells surrounded by a continuous Si-rich network, voids due to damage nucleate on the Si-rich network, propagate and finally lead to the fracture of the alloy (see green box in Fig. 1) [5,19]. The main issue with this damage mechanism is that cracks propagate quickly along this Si-rich network and can easily become too large to be healed. Damage localization particles are thus a solution of choice to maintain the damage size small enough to be healed. They are therefore introduced in the matrix (see red box in Fig. 1) in order to control the damage size and allow the PDR healing of these voids [18]. Then, healing agent should be dispersed in solid solution in the alloy (similarly to Ref. [16,20]). As discussed earlier, the supersaturated solid solution of alloying element was identified by Hautakangas *et al.* [16] as key contribution to a good healing potential. The high cooling rate of LPBF, (typically 10^6 K/s [11]) is known to increase solute trapping [21,22]. Therefore, LPBF is the technology of choice to manufacture these PDR healable Al alloys. The obtained microstructure is thus composed of α-Al cells with healing agent in solid solution surrounded by a continuous Si-rich network and damage localization particles. During an overload, void nucleation should occur by fracture and/or decohesion of the damage localization particles and not of the Si-rich network. The concept is to use a healing heat treatment (HHT) to trigger the diffusion of the healing agent and thus, allow the healing of these cavities due to damage as well as new cavities due to hydrogen blistering. However, there is a significant difference between the damage and hydrogen cavities. The cavities due to damage should contain vacuum and should therefore only be filled by the healing agent. The hydrogen cavities are already filled by hydrogen gas and require thus also the diffusion of hydrogen towards the surface, similarly to the final stage of powder sintering. In the case of a post-manufacturing heat treatment, no overload occurs and thus, no healing of the voids due to damage is expected but hydrogen blistering should be eliminated.

Therefore, to avoid hydrogen blistering in these LPBF Al-Si alloys, this work aims at tuning the composition of common 4xxx series LPBF Al alloys by addition of the high diffusion rate element Mg. Mg has indeed shown healing effect in the literature [16–18,20]. A healing agent showing a preference to precipitate on free cavities rather than in the matrix is indeed required. This will depend on different mechanisms such as the surface energy and interfacial energy between precipitates and the matrix. Moreover, Zhang *et al.* [23] showed that the atom size might also play a role. Indeed, supersaturated atoms with a radius larger than the matrix atoms will induce an increased strain energy. This induces a higher energy barrier for homogeneous nucleation in the matrix. Mg, which shows a radius 20 % larger than Al, should thus precipitate preferentially on free surfaces, filling thus the pores.

For this proof of concept, an addition of 5.5 wt% of Mg was selected in order to maximize the healing agent content and minimize the hot cracking susceptibility during LPBF [24]. This addition is supposed to lead to the precipitation of Mg_2Si damage localization particles as well as Mg in solid solution. Even if evaporation of Mg occurs during the LPBF process, a Mg content higher than the healing agent (HA) content used by Arseenko *et al.*, i.e. 3 wt% is expected. The PDR healing potential to counteract hydrogen blistering and heal voids due to damage initiated by tensile tests is thus analyzed by 3D-X-ray nano-imaging and compared to the regular AlSi12. A HHT at a temperature of 400 °C is investigated in this proof-of-concept system as it was identified by Arseenko *et al.* as the optimal PDR healing temperature [18]. Finally, an in-situ heating experiment inside TEM is performed to provide a direct confirmation of their healing potential.

2. Experimental methods

2.1. Materials

The two compositions investigated in this study are prealloyed AlSi12 and a powder mixture of AlSi12 with 5.5 wt% pure Mg. The powders used in this study are gas atomized AlSi12 powder provided by 3D Systems and pure Mg powder provided by "Société pour la Fabrication du Magnésium" (SFM). The chemical compositions of the powders, the powder mixture and the manufactured samples are provided in Table 1. Inhomogeneity due to elemental powders mixing was never observed in the manufactured parts. Due to the evaporation of Mg during LPBF, the composition will be named according to its real composition: AlSi10.5Mg4. The particle size, measured by laser diffraction granulometry in a wet dispersion (machine Coulter LS100Q), is between 6.7 μm (D10) and 35.2 μm (D90) with an average size of 22 μm for the AlSi12 powder and between 8.5 μm (D10) and 59.2 μm (D90) with an average size of 33.3 μm for the Mg powder.

2.2. Manufacturing

The LPBF equipment used in this work is the ProX200 LPBF machine from 3D Systems with a laser wavelength of 1070 nm and a laser power up to 273 W. All specimens were built on an AlSi12 substrate under argon atmosphere with a maximum oxygen content of 500 ppm. The parameters used to manufacture AlSi12 samples are the ones optimized by Gheysen *et al.* [25], i.e. laser power (P) = 164 W, scanning speed (v) = 1500 mm/s, hatching space (HS) = 70 μm and layer thickness (t) = 30 μm. The same optimization methodology was applied on AlSi12 + 5.5 wt% Mg with a new desirability criterion [25]: avoiding hot cracking. The following parameters, where hot cracking was never observed, were thus selected: P = 273 W, v = 800 mm/s, HS = 100 μm and t = 30 μm.

2.3. Characterization

In order to perform microstructural characterization, the samples were polished to mirror-like surface (0.04 μm) and the AlSi12 samples were slightly etched with a Keller reagent and were then observed by scanning electron microscopy (SEM ZEISS FEGSEM ultra 55).

To investigate the healing potential of the two selected alloys, nano-CT was performed at the European Synchrotron Radiation Facilities (ESRF Grenoble, France) on beamline ID16B, allowing to reach a voxel size of 35 nm with an energy of 17.5 keV. 2D phase contrast images of the specimen (field of view: 90 × 76 μm^2) were recorded during the sample rotation using a CMOS camera. The 3D X-ray nano-imaging was performed in-situ before and after heat treatments. A dedicated furnace can be mounted and removed on the sample to apply a heat treatment at 400 °C without moving the sample [26]. The samples were extracted on fractured tensile

Table 1
Chemical composition of the AlSi12, Mg and AlSi12 with 5.5 wt% Mg powder mixture and AlSi10.5Mg4 after LPBF in weight percentage measured by inductively coupled plasma.

	Al	Mg	Si	Ca	Fe	K	Na	Ga
AlSi12	bal.	<0.01	10.70	0.05	0.17	0.03	0.07	/
Mg	0.01	99.30	0.03	/	<0.01	/	/	0.01
AlSi12 + 5.5 wt% Mg powder mixture	84.20	5.36	10.50	/	0.10	0.03	0.03	0.01
AlSi10.5Mg4 (post LPBF)	84.60	3.96	10.50	0.03	0.15	0.04	0.03	0.01

specimen at the fracture surface and parallel to the loading direction. The tensile specimens were first polished until 300 μm thickness followed by cutting using a micro-cutting machine to reach a width of 300 μm.

After reconstruction of the scans, they were registered and segmented using the Avizo software. All the features with a size smaller than 3 voxels (0.105 μm) were considered as noise and were excluded from the analysis. The location and geometrical data of each defect such as equivalent diameter, volume and sphericity were computed.

Transmission electron microscopy (TEM) was used in order to study the healing mechanism. Broken tensile specimens were manually thinned up to around 100 μm. A disk of 3 mm diameter was cut at the fracture surface (parallel to the loading direction) in order to maximize the voids density in the sample. The disk was then further thinned and ion polished using a Gatan Duo model 691 precision ion polishing system (PIPS). The sample was observed using a FEI Osiris TEM equipped with a SuperX EDS detector in order to assess the chemical composition of determined areas. A Gatan 652 double-tilt heating holder was used for in-situ heating. High-angle annular dark-field scanning TEM (HAADF-STEM) images of the voids due to damage and an energy dispersive X-ray spectroscopy (EDS) maps were taken after 0, 1, 3 and 60 min of heating at 400 °C.

3. Results

In this section, the microstructures of the two alloys are first analyzed. Then, the damage mechanism of both investigated alloys are identified and finally, the void healing is quantified.

3.1. Microstructure

The microstructure of the AlSi12 and AlSi10.5Mg4 alloys can be observed by SEM on Fig. 2a and b, respectively. Both alloys are composed of α-Al cells surrounded by an interconnected Si-rich network. When Mg is added to AlSi12, the cellular microstructure is still observed (see Fig. 2b) but some Mg_2Si particles of 46 ± 44 nm diameter are also noticed and are embedded in the Si-rich network. Indeed, these Mg_2Si are the black particles highlighted by white arrows in Fig. 2b and identified as Mg_2Si by EDS analysis in Fig. 2c, d, e and f.

3.2. Damage mechanism

In order to understand the damage mechanism of the alloys and thus, characterize the voids due to damage sizes and compositions that need to be healed, the mid-section of fractured specimens were polished and observed by SEM, as shown in Fig. 3a and b. This surface observation confirms that damage in AlSi12 nucleates either by fracture or decohesion of the Si-rich network as discussed in literature [5].

For AlSi10.5Mg4, it is difficult to distinguish the Si-rich network and the Mg_2Si as the signal required for EDS of SEM has an interaction volume of few microns which is significantly larger than the volume of the network and the Mg_2Si particles. There is therefore a greater influence of the surrounding volume. TEM combined with EDS was thus used on a damaged AlSi10.5Mg4 sample and highlighted a change in the damage mechanism due to the Mg addition (see Fig. 3c, d, e and f). Indeed, damage does not nucleate on the Si-rich network any more but on these newly formed Mg_2Si particles following the addition of Mg to the AlSi12 alloy.

3.3. Healing potential

The voids volume due to LPBF porosities and due to damage before (see Fig. 4a and c) and after a HHT at 400 °C for 2 h (see Fig. 4b and d) was obtained using nano-CT at the ESRF for AlSi12 (see Fig. 4a and b) and AlSi10.5Mg4 (see Fig. 4c and d). The overall voids analysis is given in Table 2. It can be seen in Fig. 4c that significantly larger porosities are present in the AlSi10.5Mg4 (mean equivalent diameter of 1.4 ± 2.0 μm for AlSi10.5Mg4 and 0.8 ± 0.6 μm for AlSi12). These are attributed to the LPBF process as seen from their large and round shape which are typical of the LPBF gas pores [27]. Zhao *et al.*[19] showed that the porosity, under a certain threshold (approximately 0.5 % [19]), has a negligible influence on the damage mechanism and thus, on the static mechanical properties. These larger porosities are thus not expected to have a significant influence on the static mechanical properties.

A significant increase of the voids volume and number is observed for AlSi12 (see Fig. 4 and Table 2) while no significant effect of the heat treatment is evident for AlSi10.5Mg4. This is attributed to the commonly observed hydrogen blistering phenomenon [6]. Based on these 3D volumes (see Fig. 4), the tracking of each void was performed and the percentage of voids reduction as a function of the initial equivalent diameter is quantified (see Fig. 4e). For both alloys, the volume of small cavities decreases (smaller than 250 nm for AlSi12 and than 500 nm for AlSi10.5Mg4). However, for AlSi12, the volume of the larger cavities significantly increases (up to 45 % for the voids around 500 nm equivalent diameter) during the HHT while no significant cavity growth is evidenced for AlSi10.5Mg4.

Nano-CT offers a statistical approach of healing as it allows looking at a large number of voids, comparing size and localization (∼600 for AlSi12 and ∼350 for AlSi10.5Mg4). To determine the local healing mechanism, the evolution of a fractured Mg_2Si during HHT was observed by in-situ TEM.

Fig. 5 provides the results of this in-situ TEM analysis showing the evolution of a fractured Mg_2Si particle during a HHT at 400 °C. A significant reduction of 30 % and 44 % of the crack width is already observed after 1 and 3 min, respectively. After 1 h, the crack is completely healed, confirming that AlSi10.5Mg4 is indeed healable. Fig. 6 shows the elemental EDS maps of an Mg_2Si particle after 1 h of HHT at 400 °C. First, the chemical composition of the particle was measured: 64.5 at% Mg, 32.6 at% Si and 2.9 at% Al, confirming that this is Mg_2Si. Then, it shows that the crack is mainly filled with Al while the Mg and Si contents significantly drop down nearly to zero during the HHT (see Fig. 6e).

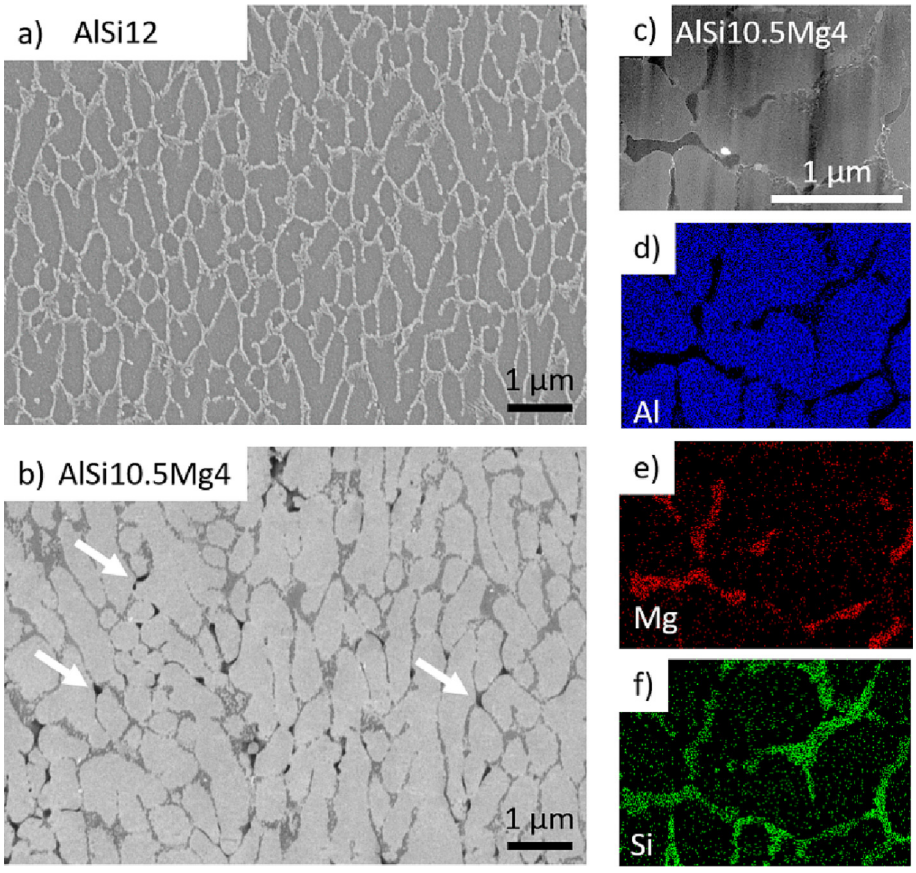

Fig. 2. SEM micrographs in secondary electron (SE) mode of a) AlSi12 (etched using Keller's reagent) and b) AlSi10.5Mg4 (no etching) where some Mg_2Si precipitates are indicated with a white arrow. c) TEM image of the microstructure of AlSi10.5Mg4 and EDS mapping analysis of the elemental composition in d) Al (in blue), e) Mg (in red) and f) Si (in green). Note that the contrast between α-Al cells and Si-rich network is inverted for AlSi12 and AlSi10.5Mg4 because AlSi12 was etched using Keller's reagent while this was not possible for AlSi10.5Mg4 due to Mg preferential etching.

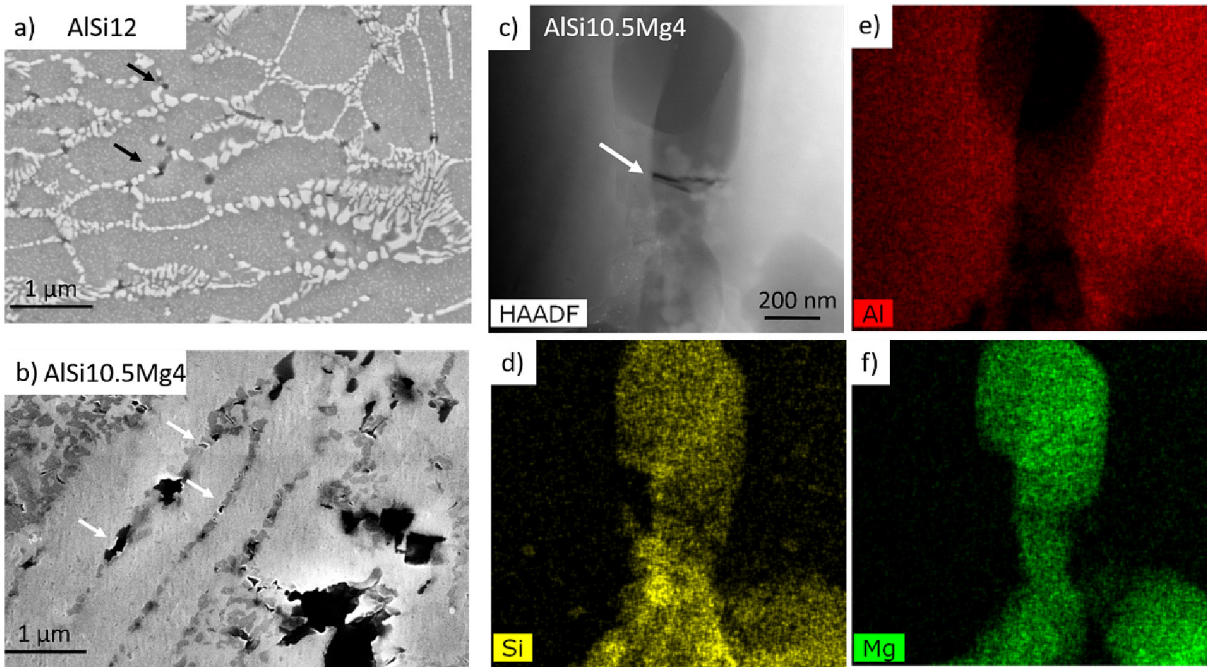

Fig. 3. SEM image of the mid-section of a fractured specimen of a) AlSi12 and b) AlSi10.5Mg4. c) TEM image of a fractured Mg_2Si particles in AlSi10.5Mg4 and its EDS elemental mapping of d) Si (in yellow), e) Al (in red) and f) Mg (in green). Arrows are drawn to highlight some damage sites. Note that the contrast between α-Al cells and Si-rich network is inverted for AlSi12 and AlSi10.5Mg4 because AlSi12 was etched using Keller's reagent while this was not possible for AlSi10.5Mg4 due to Mg preferential etching.

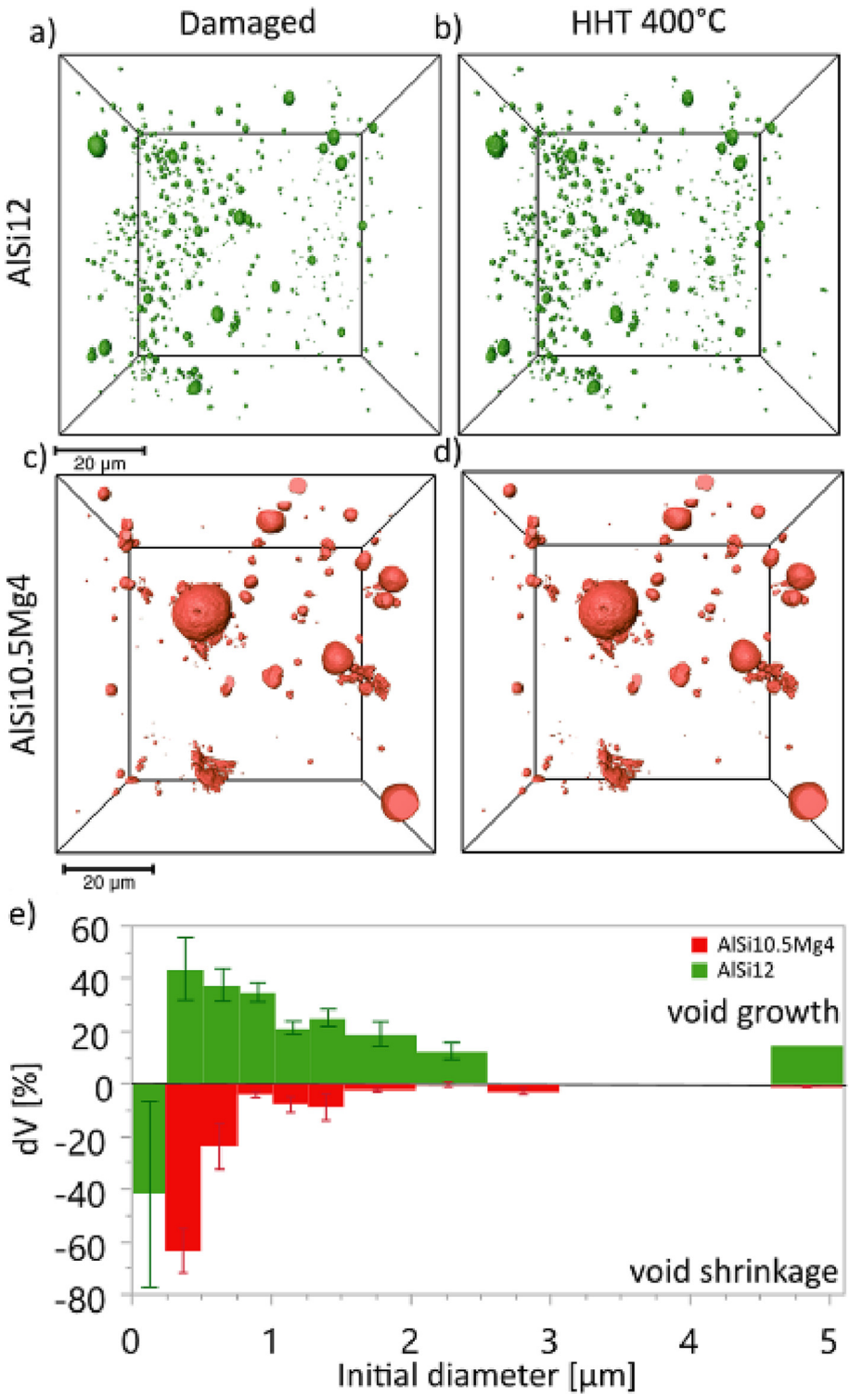

Fig. 4. Voids evolution in a) and b) AlSi12 and c) and d) AlSi10.5Mg4 samples (close to its fracture surface) a) and c) before and b) and d) after a HHT at 400 °C during 2 h in air atmosphere obtained by nano-CT at ESRF with a voxel size of 35 nm. Only the voids with a size larger than 3 voxels in diameter are represented. e) Mean percentage of voids reduction as a function of the initial equivalent diameter in the damaged AlSi12 sample (in green) and in AlSi10.5Mg4 (in red) after a HHT at 400 °C for 2 h. dV is the percentage of healed volume of a void calculated as $100\,\% \cdot (V_{healed} - V_{damaged})/V_{damaged}$. The equivalent diameter is defined as the diameter of a circle of an equal surface area. This analysis was performed manually on 200 cavities randomly selected in the volume in order to obtain a reliable statistics.

4. Discussion

AlSi12 is a commercial 4xxx series Al alloy commonly used for Laser Powder Bed Fusion (LPBF). Its microstructure is composed of α-Al cells surrounded by a Si-rich network where damage nucleates (see Fig. 3a). When a heat treatment at 400 °C during 2 h is applied, voids below 250 nm diameter significantly tend to shrink but above this size, voids grow (see Fig. 4e). This reduction of the volume of small voids can be associated to healing. 250 nm corresponds indeed to the size of the voids due to damage that were

Table 2
Global voids analysis of AlSi12 and AlSi10.5Mg4 before and after HHT at 400 °C for 2 h in air on samples of Fig. 4.

	AlSi12		AlSi10.5Mg4	
	Initial	2 h at 400 °C	Initial	2 h at 400 °C
Volume [μm^3]	577	682	350	347
Eq diameter [μm]	0.77 ± 0.02	0.80 ± 0.02	1.24 ± 0.1	1.27 ± 0.1
Sphericity	0.96	0.95	0.91	0.90
N_{voids}	609	684	87	83

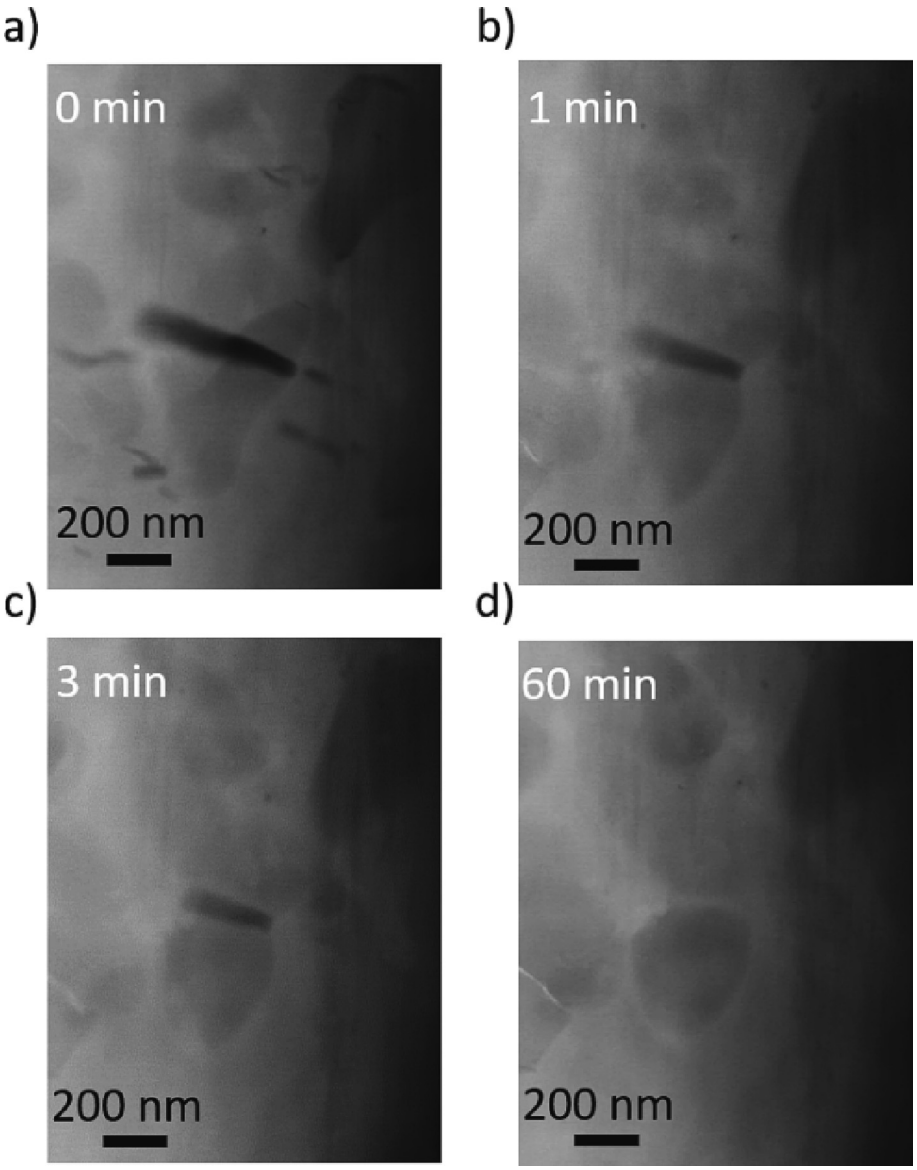

Fig. 5. STEM image of the evolution of a fractured Mg_2Si particle during a HHT at 400 °C after a) 0 min, b) 1 min, c) 3 min and d) 60 min.

healed in the Friction Stir Processed 16 passes PDR healable Al-0.5Mg_2Si [18]. This reduction could also be attributed to Ostwald ripening, i.e. dissolution of small voids which cluster on larger voids. Moreover, an increase of the global porosity volume is observed (see Table 2) which is commonly observed in Al alloys manufactured by LPBF and is attributed to hydrogen blistering as discussed in Section 1 [6].

The second composition AlSi10.5Mg4, where the fast diffusing healing agent Mg is added, is now considered. Fig. 4e shows that the voids below 500 nm shrink and that 60 % of the volume of the voids below 250 nm are filled. The healing ability seems thus to be associated to the presence of Mg. It means that the manufacturing of Programmed Damage and Repair (PDR) alloys can be achieved by LPBF, which is much more efficient and applicable to industrial parts than 16 passes of Friction Stir Processing that was proposed by Arseenko *et al.* [18].

What is really impressive in the AlSi10.5Mg4 alloy is that voids above 500 nm of equivalent diameter do not grow compared to the AlSi12. They either shrink or keep their size. Moreover, Table 2 shows a slight decrease of the voids volume and number after

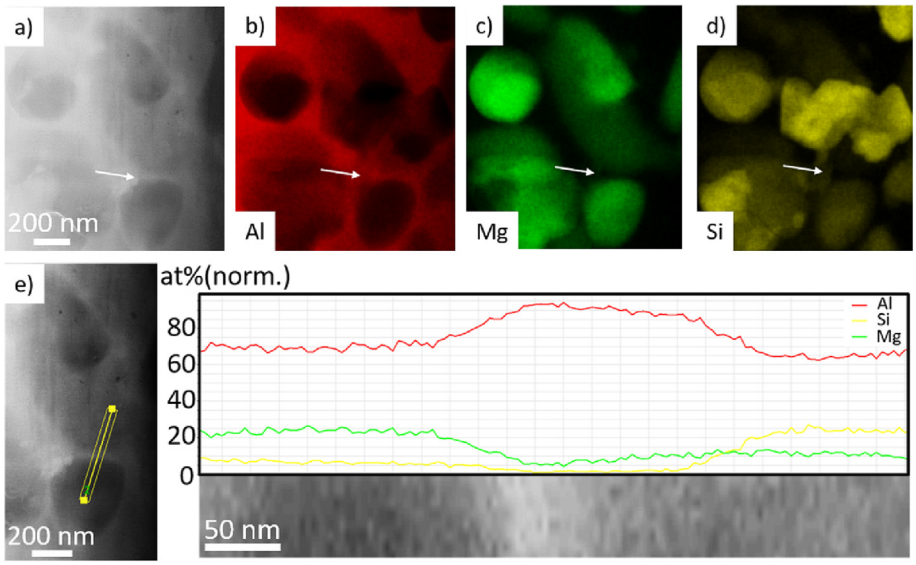

Fig. 6. Elemental composition map of a) the damaged Mg_2Si particle of Fig. 5 in b) Al, c) Mg and d) Si measured by EDS-TEM after 60 min of HHT at 400 °C. e) EDS line profile of the healed section of the Mg_2Si particle.

HHT. It seems therefore that the addition of Mg allows to counteract the porosity formation during HHT caused by the hydrogen blistering. This may be attributed to different phenomena that will now be discussed.

First, the hydrogen clustering in voids might be directly counteracted by healing of porosities thanks to the high diffusion rate Mg. This would mean that only Mg containing samples show healing. Indeed, when no Mg is present (i.e. for AlSi12 alloy), a large increase of porosity is observed.

Second, Mg could suppress or decrease the effect of H blistering observed in AlSi12. This can be due to Mg precipitation in Mg_2Si or Mg available in solid solution:

- Second phase particles and interfaces can indeed trap H atoms [28] as the solubility of H atoms can be much larger in second phases like Al_2CuMg (3 at%) than in the Al matrix (5×10^{-5} at %) [28]. However, Yamaguchi *et al.* showed that H is unstable in the lattice of Mg_2Si compared to its solution state at the tetrahedral sites in the Al matrix [29], meaning that Mg_2Si cannot trap H. This is therefore unlikely to be the root cause of the Mg efficiency.
- Mg in solid solution induces an increase of the H solubility in the α-Al matrix [30,31]. Thus, the supersaturation degree of hydrogen is reduced, leading to a decrease of H blistering, i.e. gathering of hydrogen atoms during heat treatment forming gas porosities.

In conclusion, Mg suppresses the effect of hydrogen blistering due to its healing ability and/or its influence on the H solubility in the α-Al matrix.

After this global void reduction analysis, the healing mechanism of AlSi10.5Mg4 is investigated. The AlSi10.5Mg4 is not in a stable state due to the high cooling rate of the LPBF process [6]. This triggers the presence of a highly interconnected network of Si where Mg segregates and formed fine Mg_2Si particles. Moreover, a significant amount of high diffusion rate Mg is trapped in solid solution in the α-Al cells due to the high cooling rate of LPBF [32,33]. During service life, overload induces damage nucleation either by decohesion or by fracture of these Mg_2Si damage localization particles. Then, to heal these fractured Mg_2Si particles, a high temperature is required to trigger diffusion of healing agent towards these voids [34,35]. Moreover, this healing heat treatment (HHT) increases the solubility limit of Mg leading to an increase of healing agent available. This HHT leads thus to two phenomena:

- Matrix diffusion into the crack: Indeed, the disappearance of the free surface of voids induces a decrease of the interfacial energy and thus, of the total energy of the system. Therefore, the cracks heal in order to tend to a more stable state [34,36]. This is expectedly the driving force for the healing process [18]. Notice that this migration of the atoms from the matrix towards the crack will lead to the formation of defects such as vacancies in the matrix.
- Stabilization of the microstructure: When the temperature increases above 195 °C, the supersaturated Si and Mg precipitate in the form of Mg_2Si particles [6,37]. Around 305–320 °C, the Si-rich network starts to disintegrate and globularizes on the α-Al cells boundaries while the Ostwald ripening of the fine Si precipitates leads to a coarsening of the microstructure [6,37].

It is therefore clear that Mg diffuses in the alloy during the HHT, however, it is not visible in Fig. 6 that it contributes to the healing mechanism, possibly because it is under the EDS detection limit [18]. Indeed, it is the Al matrix that diffuses towards the fractured Mg_2Si particle. No other healing mechanism observed in the PDR healable Al-0.5Mg_2Si [18] was observed in AlSi10.5Mg4. Arseenko *et al.* [18] did indeed observe two other healing mechanisms: 1) healing by matrix diffusion supported by particle's shape optimization and reconnection and 2) debonding followed by healing by surrounding material. They were just not observed on the limited selected TEM observations of the present work but are also expected to occur in AlSi10.5Mg4.

Fig. 5 shows that the crack thickness is approximately constant during the healing process while the length of the crack reduced continuously until complete healing. The healing process thus initiates from the crack tip in contact with the matrix while the interface between the crack and the Mg_2Si stays unaffected. This suggests that healing really comes from the matrix at the crack tip while the Mg_2Si globularizes, also in order to reduce its interfacial energy. Huang *et al.* [38] applied a two-dimensional finite-element method to analyze the shrinkage and splitting of microc-

racks regularly arranged on or perpendicular to a grain boundary. According to their finite-element method simulation results, this type of crack healing is characteristic of the cracks located on grain boundaries, i.e. on diffusion short-cuts [29]. Here, it is not known if the crack is located at a grain boundary, however, the Mg_2Si particles are located on the cell boundaries where a massive number of dislocations accumulate, promoting diffusion [39]. This may thus explain that the healing mechanism is similar to the grain boundary mechanism.

Healing is expected to start at the crack tip because it is a stress concentration region [40] where a high density of dislocations accumulate. This promotes therefore pipe diffusion. Moreover, Huang *et al.* [29] showed with their finite element simulation that when the dihedral angle decreases, which is the case at the crack tip, the healing rate increases.

Fig. 7 shows the healing mechanism we propose here. First, the high diffusion rate atoms Si and Mg are present in solid solution in the α-Al cells [32,33] as well as vacancies trapped in the alloy due to the high cooling rate of LPBF [41].

When the healing temperature reaches 195 °C (see Fig. 7b), the supersaturated Si precipitates in the α-Al matrix [42], meaning that the amount of Si available as healing agent drops significantly and thus, that Si might not significantly participate to the healing process.

When the healing temperature reaches 305–320 °C (see Fig. 7c), the Si-rich network starts to disintegrate and globularizes on the α-Al cells boundaries while the Ostwald ripening of the initially fine Si precipitates leads to a coarsening of the microstructure [37,42].

At 400 °C (see Fig. 7d and e), the solubility limit of Al-Mg_2Si is 0.5 at% of Mg_2Si [43], meaning that a maximum of 0.33 at% of Mg and 0.17 at% of Si are available in solid solution and thus, as healing agent while the rest of the Mg and Si form Mg_2Si precipitates. There are therefore Mg atoms in solid solution, vacancies and dislocations available at 400 °C in the matrix for diffusion healing. Goswami *et al.* [44] showed that Mg is strongly coupled to vacancies and dislocations. The high temperature activates the migration of the flux of defects towards the cells and grain boundaries, leading to an enrichment in Mg [18]. The Mg atoms can thus quickly diffuse towards the crack in order to reduce the interfacial energy. Then, the Al atoms, which are slower, follow the same short-cuts until homogenization.

5. Conclusions

A new Programmed Damage and Repair (PDR) healable Al alloy was developed by Laser Powder Bed Fusion in this work. Its healing potential was successfully highlighted using 3D X-ray nano-imaging at ESRF.

It shows that AlSi12 clearly exhibits hydrogen blistering during heat treatments. Now, its voids below 250 nm diameter significantly shrink which might be attributed to PDR healing or Ostwald ripening. However, a significant increase of the global porosity volume due to hydrogen blistering makes this potential healing of the smallest voids quite negligible.

3D X-ray nano-imaging evidenced that the addition of Mg in 4xxx series Al alloys suppresses this hydrogen blistering during heat treatments. This might be due to the presence of Mg in solid solution which increases the hydrogen solubility in the Al matrix and due to the healing of these new hydrogen gas pores. Moreover, a significant healing of voids smaller than 500 nm diameter is observed. This Mg addition also induces the precipitation of Mg_2Si

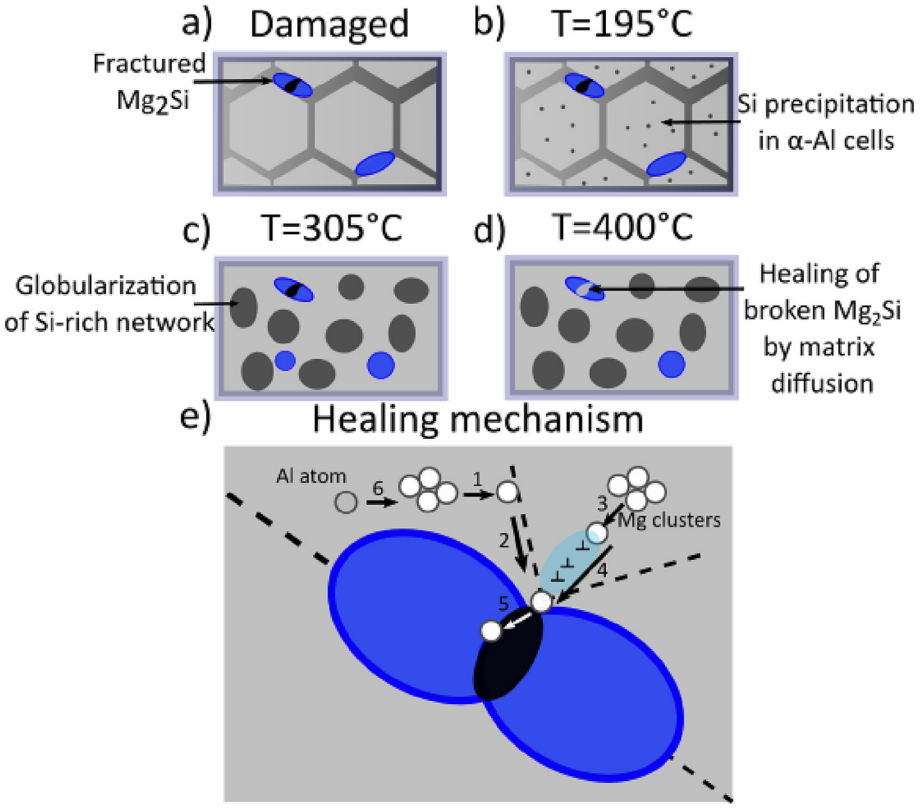

Fig. 7. Microstructure of AlSi10.5Mg4 composed of α-Al cells (light grey) surrounded by a Si-rich network (dark grey) and Mg_2Si particles (blue) a) in the damaged state and during the HHT when the temperature reaches b) 195 °C, c) 305 °C and d) 400 °C. e) Healing mechanism proposed for the AlSi10.5Mg4 alloy: 1 – diffusion of Mg atoms from clusters to grain boundaries; 2 – grain boundary diffusion of Mg atoms to the crack tip; 3 – lattice diffusion of Mg atoms to a stress field area; 4 – dislocation pipe diffusion of Mg atoms to the crack tip; 5 – diffusion of Mg atoms to a flat plane of the crack; 6 – diffusion of Al atoms through the same path as Mg atoms.

damage localization particles, required for the PDR strategy. In-situ TEM heating pointed out that the Al matrix indeed diffuses inside the fractured Mg_2Si particles, meaning that PDR healable AlSi10.5Mg4 was successfully manufactured by LPBF. This open the doors to new post-treatments to tailor mechanical properties and microstructure without hydrogen blistering as well as to new healable Al alloys manufactured by LPBF, which makes these alloys easier to build than using 16 passes of Friction Stir Processing [18].

Data availability

Data will be made available on request.

Declaration of Competing Interest

The authors declare that they have no known competing financial interests or personal relationships that could have appeared to influence the work reported in this paper.

Acknowledgements

Funding: J.G. is supported by the Fonds de la recherche scientifique – FNRS (FRIA grant), Belgium. J.G. and A.S are funded by the European Research Council (ERC) (grant agreement n °716678). H. Idrissi is mandated by the Belgian National Fund for Scientific Research (FSR-FNRS). We acknowledge the European Synchrotron Radiation Facility for provision of synchrotron radiation facilities (proposal MA4874) and we would like to thank Mariia Arseenko, Florent Hannard and Grzegorz Pyka for assistance in using beamline ID16B and for fruitful discussions. Avizo software acquisition was supported by the Fonds de la Recherche Scientifique – FNRS – EQP under grant UN06920F. The pub-lication was supported by the Fondation Universitaire de Belgique. This work was also supported by the FNRS under Grant No T.0209.23

References

[1] M. Nematollahi, A. Jahadakbar, M.J. Mahtabi, M. Elahinia, 12 – Additive manufacturing (AM), in: M. Niinomi (Ed.), Metals for Biomedical Devices (Second Edition), Woodhead Publishing, 2019, pp. 331–353.
[2] N. Kang, P. Coddet, C. Chen, Y. Wang, H. Liao, C. Coddet, Microstructure and wear behavior of in-situ hypereutectic Al–high Si alloys produced by selective laser melting, Mater. Des. 99 (2016) 120–126.
[3] J.G. Santos Macías, T. Douillard, L. Zhao, E. Maire, G. Pyka, A. Simar, Influence on microstructure, strength and ductility of build platform temperature during laser powder bed fusion of AlSi10Mg, Acta Mater. 201 (2020) 231–243.
[4] J.G. Santos Macias, Laser powder bed fusion AlSi10Mg damage and fatigue resistance improvement by post-processing, UCLouvain - Université Catholique de Louvain (2021).
[5] J.G. Santos Macías, C. Elangeswaran, L. Zhao, B. Van Hooreweder, J. Adrien, E. Maire, J.-Y. Buffière, W. Ludwig, P.J. Jacques, A. Simar, Ductilisation and fatigue life enhancement of selective laser melted AlSi10Mg by friction stir processing, Scr. Mater. 170 (2019) 124–128.
[6] P. Van Cauwenbergh, G. Krishna Muralidharan, P. Bigot, L. Thijs, B. Van Hooreweder, K. Vanmeensel, Reducing hydrogen pores and blisters by novel strategies and tailored heat treatments for Laser Powder Bed Fusion of AlSi7Mg0.6, Euro PM19, Euro PM2019, Maastricht, The Netherlands, 2019, pp. 1–7.
[7] R. Mertens, L. Baert, K. Vanmeensel, B. Van Hooreweder, Laser powder bed fusion of high strength aluminum, Mater. Des. Process. Commun. 3 (5) (2021) e161.
[8] P. Delroisse, AlSi10Mg lattice structures produced by Selective Laser Melting: from microstructure characterization to impact resistance, UCL-Université Catholique de Louvain (2018).
[9] A.J. Gerrard, Inclusions and hydrogen and their effects on the quality of direct chill cast and flat rolled aluminium alloys for aerospace applications, University of Birmingham, 2014.
[10] C. Weingarten, D. Buchbinder, N. Pirch, W. Meiners, K. Wissenbach, R. Poprawe, Formation and reduction of hydrogen porosity during selective laser melting of AlSi10Mg, J. Mater. Process. Technol. 221 (2015) 112–120.
[11] P.V. Cobbinah, R.A. Nzeukou, O.T. Onawale, W.R. Matizamhuka, Laser powder bed fusion of potential superalloys: a review, Metals 11 (1) (2021) 58.
[12] A. Schmets, G. Zaken, S. Zwaag, Self healing materials: an alternative approach to 20 centuries of materials science, 2007.
[13] M.D. Hager, P. Greil, C. Leyens, S. van der Zwaag, U.S. Schubert, Self-healing materials, Adv. Mater. 22 (47) (2010) 5424–5430.
[14] B. Grabowski, C. Tasan, Self-Healing Metals (2015).
[15] M. Arseenko, J. Gheysen, F. Hannard, N. Nothomb, A. Simar, Self-healing in metal-based systems, in: A. Kanellopoulos, J. Norambuena-Contreras (Eds.), Self-Healing Construction Materials: Fundamentals, Springer International Publishing, Cham, 2022, pp. 43–78.
[16] S. Hautakangas, H. Schut, N.H. van Dijk, P.E.J. Rivera Díaz del Castillo, S. van der Zwaag, van der Zwaag, Self-healing of deformation damage in underaged Al–Cu–Mg alloys, Scr. Mater. 58 (9) (2008) 719–722.
[17] M. Song, K. Du, S.P. Wen, Z.R. Nie, H.Q. Ye, In situ electron microscopy investigation of void healing in an Al–Mg–Er alloy at a low temperature, Acta Mater. 69 (2014) 236–245.
[18] M. Arseenko, F. Hannard, L. Ding, L.v. Zhao, E. Maire, J. Villanova, H. Idrissi, A. Simar, A new healing strategy for metals: Programmed damage and repair, Acta Mater. 238 (2022) 118241.
[19] L. Zhao, J.G. Santos Macías, L. Ding, H. Idrissi, A. Simar, Damage mechanisms in selective laser melted AlSi10Mg under as built and different post-treatment conditions, Mater. Sci. Eng. A 764 (2019) 138210.
[20] R.N. Lumley, G.B. Schaffer, Precipitation induced densification in a sintered Al–Zn–Mg–Cu alloy, Scr. Mater. 55 (3) (2006) 207–210.
[21] M.J. Aziz, J.Y. Tsao, M.O. Thompson, P.S. Peercy, C.W. White, Solute trapping: comparison of theory with experiment, Phys. Rev. Lett. 56 (23) (1986) 2489–2492.
[22] N. Takata, H. Kodaira, K. Sekizawa, A. Suzuki, M. Kobashi, Change in microstructure of selectively laser melted AlSi10Mg alloy with heat treatments, Mater. Sci. Eng. A 704 (2017) 218–228.
[23] S. Zhang, J. Kohlbrecher, F.D. Tichelaar, G. Langelaan, E. Brück, S. van der Zwaag, N.H. van Dijk, Defect-induced Au precipitation in Fe–Au and Fe–Au–B–N alloys studied by in situ small-angle neutron scattering, Acta Mater. 61 (18) (2013) 7009–7019.
[24] J. Liu, S. Kou, Susceptibility of ternary aluminum alloys to cracking during solidification, Acta Mater. 125 (2017) 513–523.
[25] J. Gheysen, M. Marteleur, C. van der Rest, A. Simar, Efficient optimization methodology for laser powder bed fusion parameters to manufacture dense and mechanically sound parts validated on AlSi12 alloy, Mater. Des. 199 (2021) 109433.
[26] J. Villanova, R. Daudin, P. Lhuissier, D. Jauffrès, S. Lou, C.L. Martin, S. Labouré, R. Tucoulou, G. Martínez-Criado, L. Salvo, Fast in situ 3D nanoimaging: a new tool for dynamic characterization in materials science, Mater. Today 20 (7) (2017) 354–359.
[27] A. Sola, A. Nouri, Microstructural porosity in additive manufacturing: The formation and detection of pores in metal parts fabricated by powder bed fusion, Journal of Advanced Manufacturing and Processing 1 (3) (2019) e10021.
[28] H. Zhao, P. Chakraborty, D. Ponge, T. Hickel, B. Sun, C.-H. Wu, B. Gault, D. Raabe, Hydrogen trapping and embrittlement in high-strength Al alloys, Nature 602 (7897) (2022) 437–441.
[29] M. Yamaguchi, T. Tsuru, K.-I. Ebihara, M. Itakura, K. Matsuda, K. Shimizu, H. Toda, Hydrogen trapping in Mg2Si and Al7FeCu2 intermetallic compounds in aluminum alloy: first-principles calculations, Mater. Trans. 61 (10) (2020) 1907–1911.
[30] H. Saitoh, Y. Iijima, Intensity of hydrogen trapping in pure Al, Al-4 wt % Cu and Al-1 wt % Mg2Si alloys measured by tritium release, J. Mater. Sci. Lett. 13 (15) (1994) 1092–1094.
[31] P.N. Anyalebechi, Analysis of the effects of alloying elements on hydrogen solubility in liquid aluminum alloys, Scr. Metall. Mater. 33 (8) (1995) 1209–1216.
[32] W. Lefebvre, G. Rose, P. Delroisse, E. Baustert, F. Cuvilly, A. Simar, Nanoscale periodic gradients generated by laser powder bed fusion of an AlSi10Mg alloy, Mater. Des. 197 (2021) 109264.
[33] X.P. Li, X.J. Wang, M. Saunders, A. Suvorova, L.C. Zhang, Y.J. Liu, M.H. Fang, Z.H. Huang, T.B. Sercombe, A selective laser melting and solution heat treatment refined Al–12Si alloy with a controllable ultrafine eutectic microstructure and 25% tensile ductility, Acta Mater. 95 (2015) 74–82.
[34] N. van Dijk, S. van der Zwaag, Self-healing phenomena in metals, Adv. Mater. Interfaces 5 (17) (2018).
[35] S. Zhang, N. van Dijk, S. Zwaag, A Review of self-healing metals: fundamentals, design principles and performance, Acta Metall. Sin. (English Letters) 33 (2020).
[36] S.H. Huo, M. Qian, G.B. Schaffer, E. Crossin, 21 – Aluminium powder metallurgy, in: R. Lumley (Ed.), Fundamentals of Aluminium Metallurgy, Woodhead Publishing 2011, pp. 655-701.
[37] J. Fiocchi, A. Tuissi, P. Bassani, C.A. Biffi, Low temperature annealing dedicated to AlSi10Mg selective laser melting products, J. Alloy. Compd. 695 (2017) 3402–3409.
[38] P. Huang, Z. Li, J. Sun, Shrinkage and splitting of microcracks under pressure simulated by the finite-element method, Metall. Mater. Trans. A 33 (4) (2002) 1117–1124.
[39] S. Min, H. Liu, M. Yang, H. Zhang, J. Hou, K. Zhang, J. Liang, J. Li, H. Wang, J. Wang, A. Huang, High-temperature oxidation performance of Ni-based GH3536 superalloy fabricated by laser powder bed fusion, npj Mater. Degrad. 6 (1) (2022) 66.

[40] Z. Balogh, G. Schmitz, 5 - Diffusion in metals and alloys, in: D.E. Laughlin, K. Hono (Eds.), Physical Metallurgy (fifth edition), Elsevier, Oxford, 2014, pp. 387–559.
[41] K. Nakamura, T. Saishoji, J. Tomioka, Grown-in defects in silicon crystals, J. Cryst. Growth 237 (2002) 1678–1684.
[42] P. Van Cauwenbergh, V. Samaee, L. Thijs, J. Nejezchlebová, P. Sedlák, A. Iveković, D. Schryvers, B. Van Hooreweder, K. Vanmeensel, Unravelling the multi-scale structure–property relationship of laser powder bed fusion processed and heat-treated AlSi10Mg, Sci. Rep. 11 (1) (2021) 6423.
[43] M. Amado, F. Daroqui, Revision of the solvus limit of Al-Mg2Si pseudo binary phase diagram, Procedia Mater. Sci. 8 (2015) 1079–1088.
[44] R. Goswami, P.S. Pao, S.B. Qadri, R.L. Holtz, Severe plastic deformation induced sensitization of cryo-milled nanocrystalline Al-7.5 Mg, Metall. Mater. Trans. A 45 (6) (2014) 2894–2898.